Journal of Computational Physics 462 (2022) 111253

Contents lists available at ScienceDirect

Journal of Computational Physics

www.elsevier.com/locate/jcp

A variational integrator for the Discrete Element Method

David N. De Klerk [a,*], Thomas Shire [a], Zhiwei Gao [a], Andrew T. McBride [a], Christopher J. Pearce [a], Paul Steinmann [a,b]

[a] Glasgow Computational Engineering Centre, James Watt School of Engineering, University of Glasgow, Glasgow G12 8QQ, United Kingdom
[b] Institute of Applied Mechanics (LTM), Friedrich-Alexander Universität Erlangen-Nürnberg (FAU), Erlangen, Germany

ARTICLE INFO

Article history:
Received 2 March 2021
Received in revised form 8 December 2021
Accepted 4 April 2022
Available online 27 April 2022

Keywords:
Discrete Element Method
Variational integrator
Quasicontinuum Method
Granular materials

ABSTRACT

A novel implicit integration scheme for the Discrete Element Method (DEM) based on the variational integrator approach is presented. The numerical solver provides a fully dynamical description that, notably, reduces to an energy minimisation scheme in the quasi-static limit. A detailed derivation of the numerical method is presented for the Hookean contact model and tested against an established open source DEM package that uses the velocity-Verlet integration scheme. These tests compare results for a single collision, long-term stability and statistical quantities of ensembles of particles. Numerically, the proposed integration method demonstrates equivalent accuracy to the velocity-Verlet method.

1. Introduction

Various descriptions of granular materials are compared in Fig. 1, where they are classified by the treatment of the temporal and spatial dimensions, which can be either continuous or discrete. In the underlying Newtonian picture (strong form), the discrete spatial degrees of freedom (particle position and orientation) are described by continuous functions of time which are the solutions to Newton's second law. The Discrete Element Method (DEM) [1] – a widely-adopted particle-level approach for simulating granular materials – calculates the resultant force acting on each particle during distinct time steps resulting from the discretisation of the time domain and solves the governing equation of motion. A continuum description (granular continuum) of spatially discrete systems is achieved via a micro-to-macro transition. For example Babic [2] proposed a coarse-graining method and derived a balance equation that relates continuous functions of position to each other. In practice, the micro-to-macro transitions for granular systems are often performed on discrete-time/discrete-space DEM data [3], but in principle this can be achieved for the Newtonian description too.

Unlike computational models of fluid dynamics or continuum mechanics, numerical simulations of granular materials have not been able take advantage of developments in spatial continuum modelling. Granular materials display a variety of behaviours which is often compared to the solid, fluid and gaseous phases of matter. The solid-like phase is characterised by static packing and jamming, the energetic gaseous state by pairwise collisions between particles, and the intermediate fluid-like state by dense flows [4]. Given the complexity and diversity of physical phenomena present in granular materials, finding a universal continuum description for granular material remains an open research question. A local continuum description for dense granular flow has been proposed [5–7] and have shown to be applicable in a range of situations. However, this rheology has limitations and fails to reproduce important non-local phenomena such as shear banding and

* Corresponding author.
E-mail address: david.deklerk@glasgow.ac.uk (D.N. De Klerk).

https://doi.org/10.1016/j.jcp.2022.111253

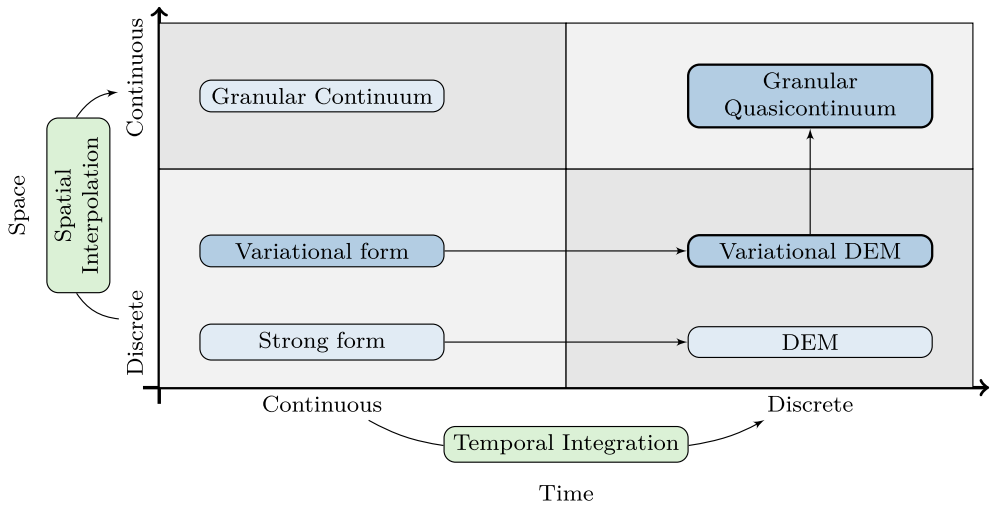

Fig. 1. A classification of descriptions of granular material based on the treatment (continuous or discrete) of the temporal and spatial dimensions. The focus of this work is a variational integrator for the Discrete Element Method which will provide the appropriate mathematical setting for a granular Quasicontinuum Method.

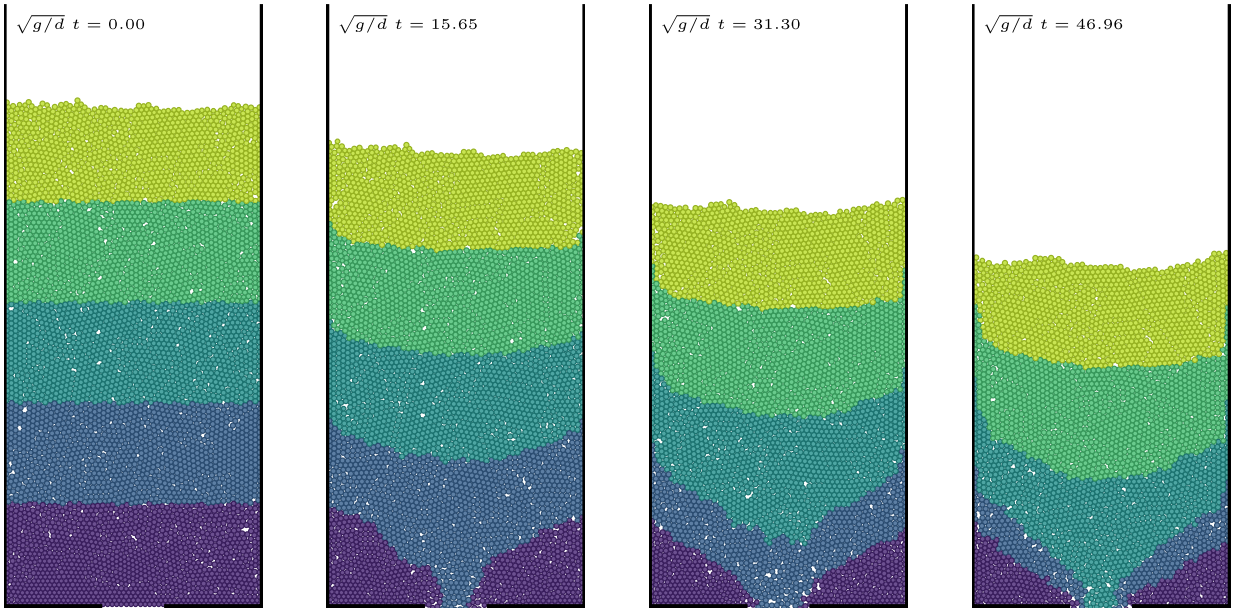

Fig. 2. A DEM simulation of a draining silo. Many particles experience only small relative displacements for the largest part of the simulation, which is common in many DEM applications.

arching [8,9]. The former occurs a granular assembly is subjected to shear loading. While there is significant particle rotation and relative motion inside the shear band the remaining part of the assembly typically moves like a rigid body [10].

In the absence of a complete continuum theory, many studies of granular materials rely on discrete, particle level numerical simulations. However, in the static or slow moving phase of granular materials, a large number of particles may remain nearly stationary or behave in a manner that could be described by a continuum model. For instance, Fig. 2 shows a draining silo with particles coloured by their initial vertical position. Even at an advanced state of drainage, particles in certain regions still approximately maintain their positions relative to their initial neighbours.

The Quasicontinuum (QC) method is a multiscale discrete-continuum method which allows for a fully-resolved particle simulation where required, and a more efficient continuum description of material behaviour elsewhere. Simulations are carried out in a continuous spatial domain and the method thus fits to the top right quadrant of the diagram in Fig. 1. The method was initially developed for crystalline atomistic simulations [11–14], where the arrangement of atoms is calculated so as to minimise the global potential energy of the system using a suitable numerical technique, such as iterative energy minimisation methods. Atoms exist throughout the domain, but the computational cost is reduced by two key features.

First, a series of representative atoms, or rep-atoms, are identified. The density of rep-atoms is highest in regions of specific interest and gradually diffuses toward regions of less interest. Second, the energy density is estimated by so-called summation rules in regions bordered by rep-atoms. The displacement of non rep-atoms is updated by interpolating their positions between rep-atoms. In situations where the majority of atoms fall in regions of low interest, the degree of freedom of the simulation is greatly reduced which leads to improved simulation run time.

The objective here is to provide a temporal discretisation framework for the application of the QC method to granular systems. However, several challenges exist before a granular QC method can be realised. For the most part, with exceptions, such as [15,16], only quasi-static configurations are simulated in the QC framework and dynamics are not accounted for. The original QC method was developed for quasi-static crystalline atomistic simulations that minimises the inter-atomic potential energy of the system. In the context of granular materials, a quasi-static simulation would restrict the method's application to the solid-like state. To recover the dynamics, and to stay consistent with the QC approach, a novel integration method for the Discrete Element Method has been developed. The method follows Hamilton's principle in seeking the stationary point of the action. The other hallmark of the QC method – an efficient summation rule – will be addressed in future work.

In a time continuous setting, Hamilton's principle provides a variational scheme where the differential equations governing a dynamical system can be derived by finding the trajectory that is the stationary point of the action. The Lagrange-d'Alembert principle is a generalisation of Hamilton's principle to non-holonomic systems, and is therefore applicable here due to the dissipative nature of granular materials. The classification in Fig. 1, identifies the Hamiltonian approach (variational) to be in the same category as the Newtonian one (strong form). Variational integrators [17–21] are a class of algorithms where the time continuous variational principles are discretised to obtain time-stepping schemes for dynamical systems. As a result, many of the important properties of Lagrangian mechanics carry over to these algorithms. For instance, variational integrators conserve the generalised momentum of a system as a consequence of a discrete version of Noether's theorem. Of particular interest is an implicit integration scheme, outlined in [19], that follows directly from Hamilton's principle in a discrete setting. When the quasi-static approximation is taken, i.e. by neglecting inertia, the method simplifies to minimising the potential energy of the system – precisely what is done in the atomistic simulations that inspired the QC method. A variational integrator for DEM is the time discrete analogue to the variational format, i.e. the time discrete description in the bottom right quadrant of Fig. 1, and provides a way to proceed towards the top right quadrant. Other variational approaches, such as the contact variational integrators [22], will be considered in future work.

While proposing variational integrators is not new per se, the bespoke application to the Discrete Element Method is novel. This is a crucial step towards a granular Quasicontinuum method. To achieve this objective, a benchmark against current DEM solvers is needed before addressing the other challenges mentioned above. The remainder of the paper is structured as follows. Section 2 provides a detailed derivation of the variational integrator for dissipative systems and extends its application to the Hookean contact model in DEM. Section 3 discusses the implementation of the solver, shows results of numerical experiments and comparisons with established DEM codes. Section 4 is dedicated to the final discussion and conclusions.

2. Numerical integration

The velocity-Verlet method [23] is popular in molecular dynamics and is also widely used in DEM. The same method is also known as the Störmer method and the leapfrog method, depending on the context where it is used [24]. It has been shown that the velocity-Verlet method and many of its variants can be derived using the variational integrator approach [24–26] and therefore inherits the properties of variational integrators mentioned in the introduction. However, the velocity-Verlet method is explicit and tailored toward solving Newton's equations in the strong form (see Fig. 1) and, as discussed above, a variational approach is preferred for the Quasicontinuum method.

In practice, DEM simulations are carried out over time periods many orders of magnitude larger than the duration of a single contact which leads to a trade off between the duration and the accuracy or stability of the simulation. To ensure accurate particle trajectories, an integration time step needs to be selected that is much smaller than the duration of a contact. Choosing the maximal integration time step has been the topic of substantial research [27–29]. Implicit integration schemes have been proposed for DEM (see for instance [30,31]). However the same limitation on the maximum time step applies, and with the added computational cost of implicit schemes these methods typically result in longer simulation times than explicit schemes. An approach to solve DEM by minimising the potential energy was proposed in [32], however this method was restricted to quasi-static configurations.

2.1. Variational integrators

The numerical integration scheme presented here follows Kane et al. [18]. The Lagrange-d'Alembert principle (see Fig. 3 (a)) is used to derive a second-order accurate integrator for the equations of motion of a general dynamical system. The continuous formulation of this principle states that for a system under the influence of a non-conservative generalised force $\boldsymbol{Q}(\boldsymbol{q}, \dot{\boldsymbol{q}})$, the sum of the variation of the action ($S = \int L\, dt$) and the total work performed by the non-conservative forces is zero, that is

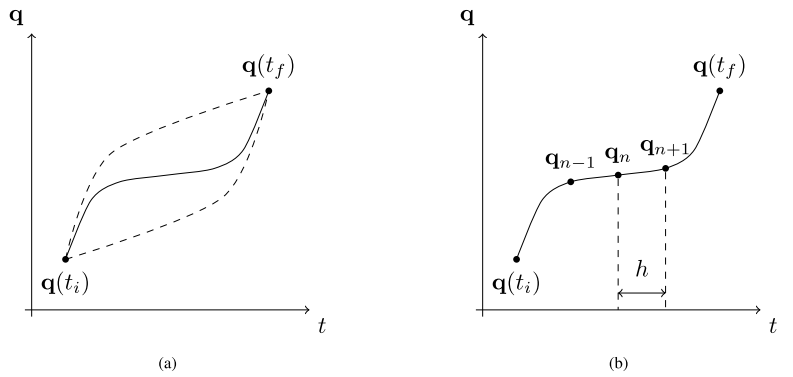

Fig. 3. Hamilton's Principle of least action, as depicted in (a), is a continuous method for solving the trajectory of a dynamical system by finding the path that is the stationary point of the action. Other possibilities are indicated by dashed lines. Variational integrators (b) in a time discretised setting, identify the sequence of points q_n that approximates the stationary point of the action.

$$\underbrace{\delta \int_{t_i}^{t_f} L(\boldsymbol{q}, \dot{\boldsymbol{q}})\, dt}_{\delta S} + \int_{t_i}^{t_f} \mathbf{Q}\,(\boldsymbol{q}, \dot{\boldsymbol{q}}) \cdot \delta \boldsymbol{q}\, dt = 0. \tag{1}$$

Here $\boldsymbol{q}$ and $\dot{\boldsymbol{q}} = d\boldsymbol{q}/dt$ are the generalised coordinates and velocities, respectively, and the Lagrangian is given by $L(\boldsymbol{q}, \dot{\boldsymbol{q}}) = T(\dot{\boldsymbol{q}}) - V(\boldsymbol{q})$, where $T(\dot{\boldsymbol{q}})$ and $V(\boldsymbol{q})$ are the kinetic and potential energy of the system, respectively.

A generalised coordinate can be any parameter that specifies the configuration of the system. For discrete particles these are the coordinates and angles that specify their position and orientation. The corresponding generalised forces are forces and torques.

In the absence of non-conservative forces ($\mathbf{Q} = \mathbf{0}$), the second term in Eq. (1) is zero and the Lagrange-d'Alembert principle is equivalent to Hamilton's principle of least action. The Lagrange-d'Alembert principle will be required to formulate an integrator for DEM, because of the dissipative terms in the contact model. Since Hamilton's principle is a special case, we will refer to it in the following discussion, when appropriate.

In order to find the trajectory that a system will follow in the time continuous case, the calculus of variations is used to find the stationary point of the action. For a time discrete formulation, the trajectory $\boldsymbol{q}(t)$ is decomposed into N time steps of length h and labelled $\{\boldsymbol{q}_0, \cdots, \boldsymbol{q}_N\}$ as depicted in Fig. 3 (b). A discrete Lagrangian is defined as the numerical approximation of the integral over the time step and is given by,

$$L_d^{\alpha}(\boldsymbol{q}_k, \boldsymbol{q}_{k+1}, h) \equiv \int_{t}^{t+h} L(\boldsymbol{q}, \dot{\boldsymbol{q}})\, dt \approx hL\left(\boldsymbol{q}_{k+\alpha}, \frac{\boldsymbol{q}_{k+1} - \boldsymbol{q}_k}{h}\right), \tag{2}$$

where $\boldsymbol{q}_{k+\alpha} = [1-\alpha]\boldsymbol{q}_k + \alpha \boldsymbol{q}_{k+1}$. The parameter α is often chosen as 0 or 1/2 which correspond to the left hand rule or midpoint rule, respectively. The choice of $\alpha = 0$ leads to a first-order accurate integrator and $\alpha = 1/2$ increases the accuracy to second-order. The discrete action is the sum over the N time steps,

$$S_d = \sum_{k=0}^{N-1} L_d^{\alpha}(\boldsymbol{q}_k, \boldsymbol{q}_{k+1}, h). \tag{3}$$

The discrete Lagrange-d'Alembert principle [18] is given by

$$\delta \sum_{k=0}^{N-1} L_d^{\alpha}(\boldsymbol{q}_k, \boldsymbol{q}_{k+1}) + \sum_{k=0}^{N-1} \left[\mathbf{Q}^{-}(\boldsymbol{q}_k, \boldsymbol{q}_{k+1}) \cdot \delta \boldsymbol{q}_k + \mathbf{Q}^{+}(\boldsymbol{q}_k, \boldsymbol{q}_{k+1}) \cdot \delta \boldsymbol{q}_{k+1} \right] = 0 \tag{4}$$

where,

$$\mathbf{Q}_d^{-}(\boldsymbol{q}_k, \boldsymbol{q}_{k+1}) = \frac{h}{2} \mathbf{Q}\left(\boldsymbol{q}_{k+\alpha}, \frac{\boldsymbol{q}_{k+1} - \boldsymbol{q}_k}{h}\right) \quad \text{and} \tag{5}$$

$$\mathbf{Q}_d^{+}(\boldsymbol{q}_k, \boldsymbol{q}_{k+1}) = \frac{h}{2} \mathbf{Q}\left(\boldsymbol{q}_{k+1-\alpha}, \frac{\boldsymbol{q}_{k+1} - \boldsymbol{q}_k}{h}\right), \tag{6}$$

are the left and right discrete forces, respectively. These terms arise from approximating the integral in the second term of (1), and applying the differential operator to the non-conservative generalised force that is a function of both the generalised

coordinates and generalised velocity, $\mathbf{Q}(\boldsymbol{q}, \dot{\boldsymbol{q}})$. A choice of $\alpha = 1/2$ corresponds to using the midpoint rule to approximate the integral and a second-order accurate integrator is achieved.

The equivalent of the Euler-Lagrange equations can be derived using Hamilton's principle of stationary action. The dynamics of the system will ensure that the variation in the action, δS_d, remains zero for independent variations in $\delta \boldsymbol{q}_k$ and $\delta \boldsymbol{q}_{k+1}$, that is

$$\delta S_d = \sum_{k=0}^{N-1} \delta \boldsymbol{q}_k \cdot \frac{d}{d\boldsymbol{q}_k} L_d^\alpha(\boldsymbol{q}_k, \boldsymbol{q}_{k+1}, h) + \sum_{k=0}^{N-1} \delta \boldsymbol{q}_{k+1} \cdot \frac{d}{d\boldsymbol{q}_{k+1}} L_d^\alpha(\boldsymbol{q}_k, \boldsymbol{q}_{k+1}, h). \tag{7}$$

To prevent confusion with derivatives, new notation is introduced such that $D_1 L_d^\alpha$ and $D_2 L_d^\alpha$ are the derivative of the first and second argument of L_d^α, respectively. Then, the index for the sum in the second term is changed to $k+1 \to k$. The expression for Eq. (7) now becomes,

$$\delta S_d = \sum_{k=0}^{N-1} \delta \boldsymbol{q}_k \cdot D_1 L_d^\alpha(\boldsymbol{q}_k, \boldsymbol{q}_{k+1}, h) + \sum_{k=1}^{N} \delta \boldsymbol{q}_k \cdot D_2 L_d^\alpha(\boldsymbol{q}_{k-1}, \boldsymbol{q}_k, h). \tag{8}$$

Since $\delta \boldsymbol{q}_0 = \delta \boldsymbol{q}_N = 0$, the first sum can start at $k = 1$ and the second can be terminated at $N-1$. Now, since both summations are carried out over the same range, the expression can be factorised, as

$$\delta S_d = \sum_{k=1}^{N-1} \delta \boldsymbol{q}_k \cdot \Big[D_1 L_d^\alpha(\boldsymbol{q}_k, \boldsymbol{q}_{k+1}, h) + D_2 L_d^\alpha(\boldsymbol{q}_{k-1}, \boldsymbol{q}_k, h) \Big]. \tag{9}$$

The condition $\delta S_d = 0$ can be enforced by requiring that the term in the brackets be zero, that is,

$$D_1 L_d^\alpha(\boldsymbol{q}_k, \boldsymbol{q}_{k+1}, h) + D_2 L_d^\alpha(\boldsymbol{q}_{k-1}, \boldsymbol{q}_k, h) = \mathbf{0}, \tag{10}$$

which is the discrete form of the Euler-Lagrange equation.

In the general case when dissipative forces are present (i.e. $\mathbf{Q} \neq \mathbf{0}$), the second term in Eq. (4) can be manipulated using the same steps as above to obtain,

$$\sum_{k=0}^{N-1} \Big[\mathbf{Q}_d^-(\boldsymbol{q}_k, \boldsymbol{q}_{k+1}, h) \cdot \delta \boldsymbol{q}_k + \mathbf{Q}_d^+(\boldsymbol{q}_k, \boldsymbol{q}_{k+1}) \cdot \delta \boldsymbol{q}_{k+1} \Big] = \sum_{k=1}^{N-1} \delta \boldsymbol{q}_k \cdot \Big[\mathbf{Q}_d^-(\boldsymbol{q}_k, \boldsymbol{q}_{k+1}, h) + \mathbf{Q}_d^+(\boldsymbol{q}_{k-1}, \boldsymbol{q}_k) \Big]. \tag{11}$$

The sum over k and $\delta \boldsymbol{q}_k$ can be factored with the terms in (9), which leads to the discrete Euler-Lagrange equation,

$$D_1 L_d^\alpha(\boldsymbol{q}_k, \boldsymbol{q}_{k+1}, h) + D_2 L_d^\alpha(\boldsymbol{q}_{k-1}, \boldsymbol{q}_k, h) + \mathbf{Q}_d^-(\boldsymbol{q}_k, \boldsymbol{q}_{k+1}, h) + \mathbf{Q}_d^+(\boldsymbol{q}_{k-1}, \boldsymbol{q}_k, h) = \mathbf{0}. \tag{12}$$

Both Eqs. (10) and (12) are second-order difference equations, but a system of two first-order equations can be constructed by introducing the generalised momentum. The momentum in the time continuous case is defined by, $\boldsymbol{p}(t) = \partial L / \partial \dot{\boldsymbol{q}}$. Similarly in the time discrete setting, the momentum at step k is given by

$$\boldsymbol{p}_k \equiv D_2 L_d^\alpha(\boldsymbol{q}_{k-1}, \boldsymbol{q}_k, h). \tag{13}$$

The momentum can be used to evaluate $\mathbf{Q}^+$ at time step k,

$$\mathbf{Q}_d^p(\boldsymbol{q}_k, \boldsymbol{p}_k) = \frac{h}{2} \mathbf{Q}\left(\boldsymbol{q}_k, \frac{\boldsymbol{p}_k}{m}\right) = \mathbf{Q}^+(\boldsymbol{q}_{k-1}, \boldsymbol{q}_k, h). \tag{14}$$

The first update equation is obtained by substituting the definition for the momentum (13) at step k, into the discrete Euler-Lagrange equation (12), and the second is the expression for the momentum at step $k+1$. The pair of first-order update equations is given by,

$$\boldsymbol{R}(\boldsymbol{q}_k, \boldsymbol{q}_{k+1}, \boldsymbol{p}_k, h) \equiv \boldsymbol{p}_k + D_1 L_d^\alpha(\boldsymbol{q}_k, \boldsymbol{q}_{k+1}, h) + \mathbf{Q}_d^-(\boldsymbol{q}_k, \boldsymbol{q}_{k+1}, h) + \mathbf{Q}_d^p(\boldsymbol{q}_k, \boldsymbol{p}_k) = \mathbf{0}, \tag{15}$$

$$\boldsymbol{p}_{k+1} = D_2 L_d^\alpha(\boldsymbol{q}_k, \boldsymbol{q}_{k+1}, h). \tag{16}$$

The update scheme, $(\boldsymbol{q}_k, \boldsymbol{p}_k) \mapsto (\boldsymbol{q}_{k+1}, \boldsymbol{p}_{k+1})$, requires that the new position, $\boldsymbol{q}_{k+1}$ be calculated using an implicit scheme in Eq. (15) and then explicitly calculating the new momentum $\boldsymbol{p}_{k+1}$ using (16).

The implicit scheme for updating $\boldsymbol{q}$ is obtained by expanding (15) around $\boldsymbol{q}_{k+1}$,

$$\boldsymbol{R}(\boldsymbol{q}_k, \boldsymbol{q}_{k+1}^n, \boldsymbol{p}_k, h) + \mathbf{K}(\boldsymbol{q}_k, \boldsymbol{q}_{k+1}^n, \boldsymbol{p}_k, h) \Delta \boldsymbol{q}_{k+1}^n = \mathbf{0}, \tag{17}$$

where $\boldsymbol{q}_{k+1}^n$ is the previous estimate for $\boldsymbol{q}_{k+1}$ and $\Delta\boldsymbol{q}_{k+1}^n = \boldsymbol{q}_{k+1}^{n+1} - \boldsymbol{q}_{k+1}^n$ is the change required to improve the estimate. The stiffness is given by,

$$\mathbf{K}(\boldsymbol{q}_k, \boldsymbol{q}_{k+1}, h) = \frac{\partial}{d\boldsymbol{q}_{k+1}} \boldsymbol{R}(\boldsymbol{q}_k, \boldsymbol{q}_{k+1}, h) \tag{18}$$

$$= \frac{\partial^2}{\partial \boldsymbol{q}_k \partial \boldsymbol{q}_{k+1}} L_d^{\alpha}(\boldsymbol{q}_k, \boldsymbol{q}_{k+1}, h) + \frac{\partial}{\partial \boldsymbol{q}_{k+1}} \boldsymbol{Q}_d^{-}(\boldsymbol{q}_k, \boldsymbol{q}_{k+1}, h) \tag{19}$$

The initial guess for $\boldsymbol{q}_{k+1}$ can be estimated using the momentum at the k-th time step, $\boldsymbol{q}_{k+1}^0 = \boldsymbol{q}_k + h\boldsymbol{p}_k/m$. A sequence of improvements $n = 1, 2\ldots$ is computed until a new set of generalised coordinates are reached where the magnitude of the residual $\boldsymbol{R}$ is zero to within a specified tolerance.

2.2. Integration for DEM

DEM is characterised by treating particles as rigid bodies with 'soft' contacts where overlap between particles is allowed and inter-particle forces are expressed as a function of the overlap (denoted by δ_{ij}). Different contact models have been proposed (for instance see [33] for a recent review), but for simplicity and without loss of generality the Hookean contact model [33,34] is adopted. Specifically, the normal and tangential forces between particles, expressed in the global coordinate system, are calculated using

$$\boldsymbol{F}_{n_{ij}} = k_n \delta_{ij} \boldsymbol{n}_{ij} - \gamma_n m_{\text{eff}} \boldsymbol{v}_{n_{ij}}, \tag{20}$$

$$\boldsymbol{F}_{t_{ij}} = k_t \delta_{ij} \boldsymbol{t}_{ij} - \gamma_t m_{\text{eff}} \boldsymbol{v}_{t_{ij}}, \tag{21}$$

where k_n and k_t are the normal and tangential spring stiffness, γ_n and γ_t are the normal and tangential damping coefficients and $m_{\text{eff}} = m_i m_j/[m_i + m_j]$ is the effective mass of the contact. The overlap, normal and tangential components of the velocity, are given by,

$$\boldsymbol{v}_{n_{ij}} = \left[\boldsymbol{v}_{ij} \cdot \boldsymbol{n}_{ij}\right] \boldsymbol{n}_{ij}, \tag{22}$$

$$\boldsymbol{v}_{t_{ij}} = \boldsymbol{v}_{ij} - \boldsymbol{v}_{n_{ij}} - \frac{1}{2}\left[\boldsymbol{\omega}_i + \boldsymbol{\omega}_j\right] \times \boldsymbol{r}_{ij}, \tag{23}$$

respectively, where $\boldsymbol{r}_{ij} = \boldsymbol{r}_i - \boldsymbol{r}_j$ is the relative position of the particles, $\boldsymbol{n}_{ij} = \boldsymbol{r}_{ij}/|\boldsymbol{r}_{ij}|$ is the unit vector normal to the contact, $\boldsymbol{t}_{ij}$ is unit vector tangential to the contact, $\delta_{ij} = d - |\boldsymbol{r}_{ij}|$ is the overlap between the particles with diameter d, $\boldsymbol{v}_{ij} = \boldsymbol{v}_i - \boldsymbol{v}_j$ is the relative velocity and $\boldsymbol{\omega}$ is the angular velocity.

The dynamics of particle i is governed by the resultant force and torque,

$$\boldsymbol{F}_i = \boldsymbol{F}_i^{\text{ext}} + \sum_j \left[\boldsymbol{F}_{n_{ij}} + \boldsymbol{F}_{t_{ij}}\right], \tag{24}$$

$$\boldsymbol{\tau}_i = -\frac{1}{2}\sum_j \left[\boldsymbol{r}_{ij} \times \boldsymbol{F}_{t_{ij}}\right], \tag{25}$$

where $\boldsymbol{F}_i^{\text{ext}}$ are any external forces on particle i and the sum j is carried out over all particles that are in contact with i, i.e. for which $\delta_{ij} > 0$.

The DEM method can be cast into the Lagrangian formulation where the Lagrangian for a system of N_p discrete particles is given by,

$$L(\boldsymbol{q}, \dot{\boldsymbol{q}}) = \frac{1}{2}\dot{\boldsymbol{q}}^T \mathbf{M} \dot{\boldsymbol{q}} - V(\boldsymbol{q}), \tag{26}$$

where $\boldsymbol{q}$ is a $6N_p$ real column vector that represents the degrees of freedom of all N_p particles. The integrator needs to account for the position and orientation of each particle, so a reasonable choice is to group the vector in rows of 6, where the first 3 entries and last 3 entries represent the position and angular degrees of freedom, respectively. As before, the generalised velocity is $\dot{\boldsymbol{q}} = d\boldsymbol{q}/dt$ which is therefore composed of the linear and angular velocity. The generalised momentum, $\boldsymbol{p}$, contains both the linear and angular momentum. A component of $\boldsymbol{p}$ is given by $p = \partial L/\partial \dot{q}$, where $\dot{q}$ is the corresponding component of $\dot{\boldsymbol{q}}$. The mass matrix $\mathbf{M}$ is a $6N_p \times 6N_p$ diagonal matrix with blocks $\mathbf{M}_i = \text{diag}([m_i\ m_i\ m_i\ I_i\ I_i\ I_i])$. Here m_i and I_i are the particle mass and moment of inertia, respectively, of particle i.

The first term in Eq. (26) accounts for the total kinetic energy of the system. The potential energy due to a Hookean contact between particles i and j is given by

$$V_{ij} = \begin{cases} \frac{k_n}{2}\left[\delta_{ij}\right]^2, & \text{if } \delta_{ij} > 0 \\ 0, & \text{otherwise.} \end{cases} \tag{27}$$

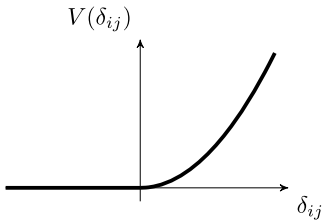

Fig. 4. The Hookean inter-particle potential function as a function of particle overlap.

The potential function is illustrated in Fig. 4. This formulation can be expanded to other contact models, for instance a Hertz-Mindlin contact model can be implemented by using $V_{ij} \propto 2/5\ [\delta_{ij}]^{5/2}$ for $\delta_{ij} > 0$. The potential energy for the entire system is the sum of the potentials over all the particles in contact with each other and, assuming a gravitational acceleration $\boldsymbol{g} \hat{=} [0, 0, -g]$, the gravitational potential energy $V = \sum_i \sum_{j<i} V_{ij} + \sum_i m_i g z_i$. The generalised non-conservative forces $\boldsymbol{Q}$ in DEM are friction and velocity dependent damping terms in Eqs. (20)-(21).

Following the prescription in Eq. (2), the discrete Lagrangian for DEM is given by,

$$L_d^{\alpha}(\boldsymbol{q}_k, \boldsymbol{q}_{k+1}, h) = \frac{1}{2h}\left[\boldsymbol{q}_{k+1} - \boldsymbol{q}_k\right]^T \mathbf{M}\left[\boldsymbol{q}_{k+1} - \boldsymbol{q}_k\right] - hV(\boldsymbol{q}_{k+\alpha}). \tag{28}$$

This allows one to simplify the update scheme for the integrator. The vector term in Eq. (17) becomes,

$$\boldsymbol{R}(\boldsymbol{q}_k, \boldsymbol{q}_{k+1}^n, \boldsymbol{p}_k, h) = \boldsymbol{p}_k - \frac{1}{h}\mathbf{M}\left[\boldsymbol{q}_{k+1}^n - \boldsymbol{q}_k\right] - h\left[[1-\alpha]\frac{\partial V}{\partial \boldsymbol{q}_k} + \frac{1}{2}\boldsymbol{Q}^{-}(\boldsymbol{q}_k, \boldsymbol{q}_{k+1}^n) + \frac{1}{2}\boldsymbol{Q}^{p}(\boldsymbol{q}_k, \boldsymbol{p}_k)\right], \tag{29}$$

and the stiffness matrix,

$$\mathbf{K}(\boldsymbol{q}_k, \boldsymbol{q}_{k+1}^n, h) = -\frac{1}{h}\mathbf{M} - \frac{\partial}{\partial \boldsymbol{q}_{k+1}}\boldsymbol{Q}_d^{-}(\boldsymbol{q}_k, \boldsymbol{q}_{k+1}, h). \tag{30}$$

Using these expressions for $\boldsymbol{R}$ and $\mathbf{K}$ in the iterative scheme described in equation (17), the generalised coordinates of the system can be calculated at the next time step. The time step size h plays an important role in regulating the step size of the position i.e. $|\Delta \boldsymbol{q}_{k+1}^n|$. When h is not sufficiently small the scheme may not converge. This can be mitigated by using a suitable time step or with techniques commonly used in nonlinear problems such as where the convergence radius of the Newton scheme can be improved using arc length control methods.

The momentum update equation (16) simplifies to

$$\boldsymbol{p}_{k+1} = D_2 L_d^{\alpha} = \frac{1}{h}\mathbf{M}[\boldsymbol{q}_{k+1} - \boldsymbol{q}_k] - h\alpha\frac{dV}{dq_k}. \tag{31}$$

For the first-order integrator ($\alpha = 0$), this can be interpreted as the product of the discrete velocity and the mass and is therefore consistent with a discrete time increment.

3. Numerical tests

The integration scheme outlined above is implemented in the Python programming language [35,36]. The complete algorithm is outlined in Algorithm 1 and the full source code is available online [37]. The iterative scheme for computing the next position is terminated when the norm of the residual or position update is reduced to 10^{-13} of their respective initial values. A message is posted to the user when neither of these conditions are met after 200 iterations, which indicates that a smaller time step would yield more accurate results. A Verlet neighbour list [23] efficiently keeps track of potential contacts and assists in constructing the residual vector and stiffness matrix. To simplify the implementation and to focus on key features of the algorithm, the tangential overlap between particles is not calculated which restricts the following numerical tests to frictionless particles ($\mu = 0$), however dissipative forces are still present via viscous damping and accounted for by the second terms in equations (20)-(21).

Walls are implemented using the Hookean contact model Eqs. (20)-(21) by substituting the position $\boldsymbol{r}_j$ with the wall's normal vector and setting $\boldsymbol{v}_j = \mathbf{0}$.

A number of numerical experiments are performed to test the integrator and its implementation. Fig. 5 shows the various configurations used in the tests: a collision between two particles, a single particle bouncing between two parallel walls, a collision between a bonded pair and a third particle, and an ensemble of particles settling in a box under gravity. Each case is discussed in the following sections. In each test case all particles have the same diameter and mass and the same parameters for the Hookean contact model with no friction ($\mu = 0$) and normal and tangential damping is fixed to $\gamma_t = \gamma_n/2$. A damping parameter is introduced $\gamma = \gamma_n/m_{\text{eff}}$, and different values of the parameter γ are used to test

Read initial state;
Assemble $\mathbf{M}$;
$k \leftarrow 0$;
while $k < K$ **do**
  Detect Contacts;
  $\boldsymbol{q}_{k+1}^0 \leftarrow \boldsymbol{q}_k + h\mathbf{M}^{-1}\boldsymbol{p}_k$; /* The initial guess for the position */
  $n \leftarrow 0$;
  while $n < 200$ **do**
    $\boldsymbol{F} \leftarrow$ Vector term in (29);
    $\mathbf{K} \leftarrow$ Matrix term in (30);
    $\Delta\boldsymbol{q}_{k+1}^{\Delta n} \leftarrow CG(\mathbf{K}, -\boldsymbol{F}, \text{tol} = 10^{-15})$; /* Solve with the conjugate gradient method */
    $\boldsymbol{q}_{k+1}^{n+1} \leftarrow \boldsymbol{q}_{k+1}^{n} + \Delta\boldsymbol{q}_{k+1}^{\Delta n}$; /* Update the guess for the next iteration */
    $d_n \leftarrow |\Delta\boldsymbol{q}_{k+1}^{\Delta n}|$;
    $E_n \leftarrow |F|$;
    if *n == 0* **then**
      $d_0 \leftarrow d_n$;
      $E_0 \leftarrow E_n$;
    if $E_n/E_0 < 10^{-13}$ **or** $E_n/E_0 < 10^{-13}$ **then**
      break from inner loop;
    $n \leftarrow n + 1$;
  if *n == 200* **then**
    print "Maximum Newton iterations reached" ;
  $\boldsymbol{q}_{k+1} \leftarrow \boldsymbol{q}_{k+1}^{n}$; /* Set the coordinates for the next iteration */
  $\boldsymbol{p}_{k+1} \leftarrow \frac{1}{h}\mathbf{M}\left[\boldsymbol{q}_{k+1} - \boldsymbol{q}_k\right]$; /* Update the momentum using Eq. (31) */
  $k \leftarrow k + 1$;

Algorithm 1: The first-order ($\alpha = 0$) variational integrator algorithm for DEM.

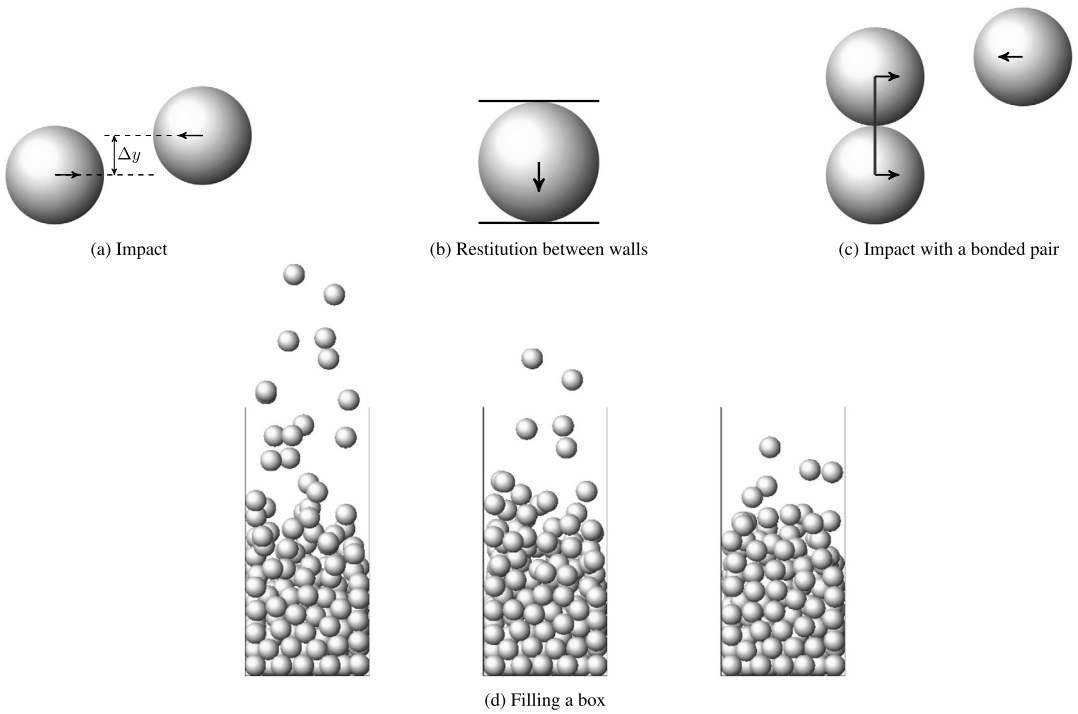

(a) Impact (b) Restitution between walls (c) Impact with a bonded pair

(d) Filling a box

Fig. 5. Particle configurations used for numerical experiments in this section: (a) collision between two particles, (b) a particle bouncing between walls, (c) collision with simplified bonded particles and (d) particles filling a box. Solid lines between particle centres indicate that a simplified 'bond' was present between particles.

various aspects of the integrator. In all simulations the value of the contact stiffness is fixed relative to other model parameters such that $kd/mg = 195\,000$, where g is gravitational acceleration and m and d are the particle mass and diameter, respectively.

The algorithm outlined above provides an integrator for DEM in a variational setting. In order to demonstrate that it indeed recovers the same solution as a conventional DEM simulation, comparisons are made with the results from the

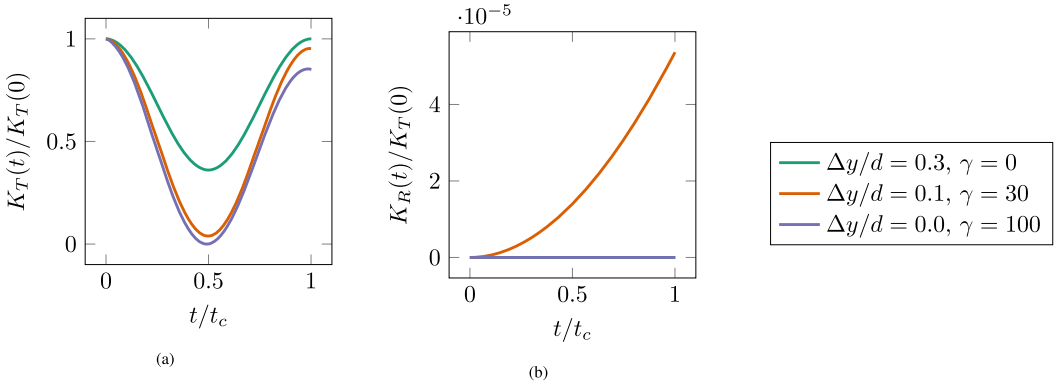

Fig. 6. Two particle impact: Kinetic energy of one particle for small integration time steps ($h \approx t_c/160$) and various parameters. Results between the proposed integrator and LAMMPS are indistinguishable. (For interpretation of the colours in the figures, the reader is referred to the web version of this article.)

open source software package LAMMPS [38], where possible. LAMMPS implements a Hookean contact model [34,39,40]. The default velocity-Verlet [23] integrator in LAMMPS is used, which is a popular choice for DEM simulations and readily implemented in other open source packages [41]. The current version of LAMMPS only provides two integrators for fully dynamical simulations, the other being the rRESPA [42] multi-timescale scale integrator. The velocity-Verlet scheme was chosen, because only inter-particle forces are considered here.

3.1. Two particle impact

The first test shows the numerical integration of the Hookean contact model over one collision between two particles. Simulations for different values of the integration time step h, damping γ and offset Δy (see Fig. 5a) are performed. The two particles have initial positions $\boldsymbol{r} \hat{=} [d, \pm\Delta y/2, 0]$ and velocities $\boldsymbol{v} \hat{=} [\mp v, 0, 0]$.

An analytical solution is available for the special case when $\Delta y = 0$, as all contributions from tangential forces remain zero. The time at which the collision starts can be calculated and is given by $t_A = d/2v$. After this time, the force between the particles is given by

$$F = k_n[d - x] + \frac{1}{2}\gamma m v, \tag{32}$$

where $[x, 0, 0]$ and $[-v, 0, 0]$ is the position and velocity, respectively, of the particle on the right. This is the same force as a damped simple harmonic oscillator for which the position and velocity are given by:

$$x(t) = \frac{d}{2} - v t_\gamma \exp\left(-\frac{\gamma\, t}{m}\right) \sin\left(\frac{t}{t_\gamma}\right), \tag{33}$$

$$v(t) = v \exp\left(-\frac{\gamma t}{m}\right)\left[\frac{\gamma^2}{m}\sin\left(\frac{t}{t_\gamma}\right) - \cos\left(\frac{t}{t_\gamma}\right)\right], \tag{34}$$

where $t_\gamma = \left[2k/m - [\gamma/m]^2\right]^{-1/2}$. The duration of the collision can also be calculated by solving for t in $x(t) = d/2$, which gives $t_C = \pi\sqrt{m/(2k)}$.

Figs. 6 to 8 show the translational and rotational kinetic energy of the particle on the right over the course of the collision. The translational kinetic energy was calculated as $K_T = 1/2\ m[v_x^2 + v_y^2]$, where $\boldsymbol{v} \hat{=} [v_x, v_y, 0]$ is the particle velocity, and rotational kinetic energy $K_R = 1/2\ I\omega_z^2$, where $I = 2/5\ m[d/2]^2$ is the moment of inertia of a sphere and ω_z is the rotational velocity around the z axis. Figs. 6a and 6b shows results of the proposed integrator for a small time step $h \approx t_c/160$. For this time step size there is excellent agreement with LAMMPS and results between the two integrators are indistinguishable. Comparisons between the first and second-order integrators and LAMMPS at larger time steps ($h \approx t_c/3.2, t_c/16.1$, $\Delta y/d = 0.1$ and $\gamma = 30$) are made in Fig. 7a and 7b. The second-order integrator compares well with LAMMPS in the case when $h = t_c/16.1$, but the amount of energy dissipated is (not surprisingly) incorrectly calculated for large time steps $h = t_c/3.2$ by all integrators tested. Finally, Fig. 8 compares the second-order integrator (with $h \approx t_c/160$ and $\Delta y = 0$) to the analytic solution in equation (34) and demonstrates near exact agreement.

The stability of the variational integrator can be tested numerically using the analytic solution. However, the velocity-Verlet method's stability interval is larger than the duration of a single collision [43]. To make meaning full comparisons, the contact force was altered to $V(\delta_{ij}) = k/2\delta_{ij}$, $\forall\delta_{ij}$ so that the inter-particle force becomes attractive when the particles separate. The two particles were initially placed at $\boldsymbol{r} \hat{=} [\pm d/2, 0, 0]$, such that $\delta_{ij} = 0$ at $t = 0$, and given the same initial

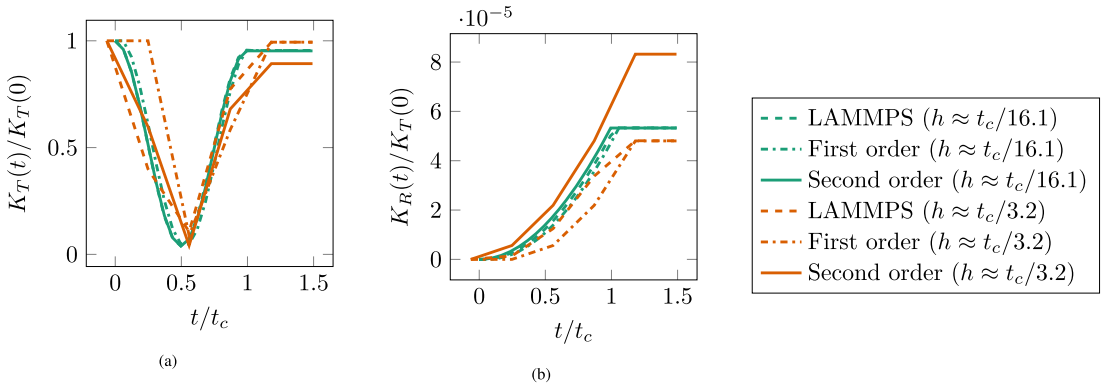

Fig. 7. Two particle impact: Kinetic energy of one particle for large integration time steps ($h \approx t_c/3.2, t_c/16.1$) and $\Delta y/d = 0.1$ and $\gamma = 30$. There is agreement between LAMMPS and the second-order integrator for $h \approx t_c/16.1$, but the energy dissipation over the course of the collision is not correctly calculated for the very large time step $h \approx t_c/3.2$.

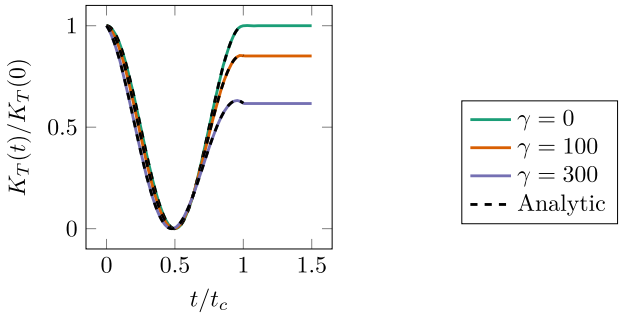

Fig. 8. Two particle impact: Kinetic energy of one particle ($h \approx t_c/160$, $\Delta y = 0$) compared to the analytic solution in equation (34).

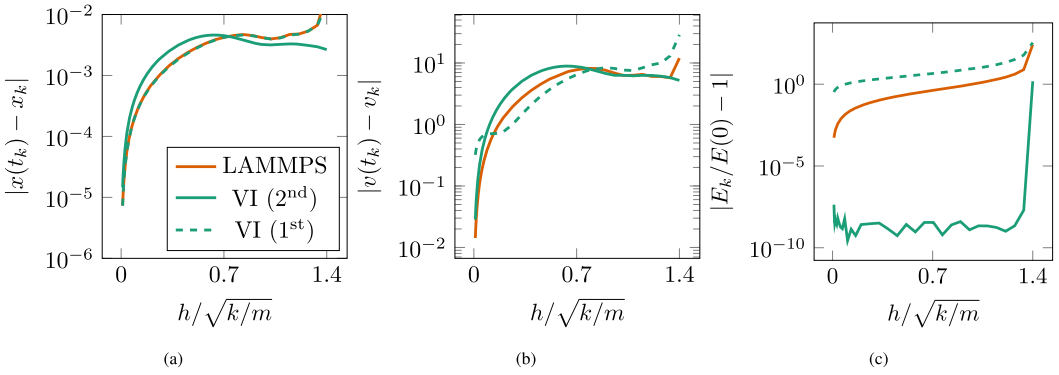

Fig. 9. For the example of a two particle impact with the modified 'bonded' contact model the numerical error in (a) position (b) velocity and (c) total energy. The second-order method's position and velocity is less accurate than the velocity-Verlet method, but the total energy remains conserved to within numerical precision. The first-order method calculates the same position as the velocity-Verlet method, but accuracy suffers for the velocity.

velocities as in the previous example, $\boldsymbol{v} \triangleq [\mp v, 0, 0]$. This example is analogous to the harmonic oscillator and the analytic solution in (33) and (34) is valid for all $t > 0$, however it should be noted that in this example the overlap between particles δ_{ij} only accounts for half of the displacement of a particle. Therefore, the angular frequency of an analogous harmonic oscillator would be $\sqrt{2k/m}$. With these parameters the stability interval of the velocity-Verlet method is expected to be $h < \sqrt{2m/k}$ instead of $h < 2\sqrt{m/k}$ that is typically reported in literature for the harmonic oscillator.

A series of simulations were performed with different time steps in $h \in [0.01\sqrt{m/k}, 1.4\sqrt{m/k}]$ using the first and second-order variational integrators and the velocity-Verlet method in LAMMPS. The error in position, velocity and kinetic energy was calculated as the L^2 norm of the difference between the numerical solution and the analytic solution evaluated at the same time steps. For instance, the error in position can be calculated using $e_x = |x_k - x(t_k)|$. The errors vs time step for position, velocity and total energy are shown in Fig. 9. The first-order method predicts the same positions as the velocity-Verlet

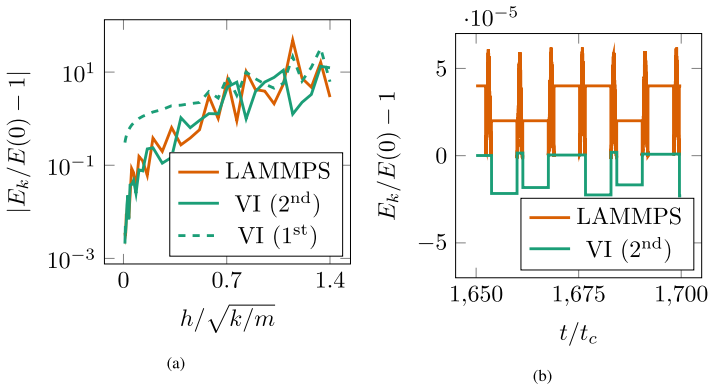

Fig. 10. For a particle bouncing between two walls $1.01d$ apart (a) shows the numerical error vs time step. The performance of the second-order variational integrator suffers in the presence of discontinuities in the derivative of the contact model, but still outperforms the first-order method and performs similar to the velocity-Verlet scheme. The truncation error in the total energy vs time is shown in (b).

method, however the accuracy of the velocity does not improve as rapidly as the second-order methods when the time step is reduced. The second-order method produces less accurate positions and velocity, however the accuracy improves at a similar rate to the velocity-Verelet method. In addition the total energy is conserved for $h\sqrt{k/m} < \sqrt{2}$ to within the tolerance specified for the conjugate gradient method.

3.2. Particle bouncing between walls

Variational integrators are known to display excellent energy conservation, despite the fact that energy conservation is not guaranteed [18], and this has been demonstrated in the previous example. However, the presence of collisions, and given that the Hookean contact model has a discontinuous second derivative, a reduction in accuracy in realistic DEM simulations may occur. To test the energy conservation behaviour of the variational integrator, a simulation is performed where a particle is placed between two parallel walls set $1.01d$ apart. The particle's initial velocity is perpendicular to them (see Fig. 5b). In the undamped case ($\gamma_t = \gamma_n = 0$), the particle will bounce between the walls without loss of energy and thereby provide a good test for the energy conserving properties of the integrator. During the brief periods of no contact the total energy in the system will be the particle's kinetic energy and during a collision some energy will be converted to potential energy $V = 1/2\ k_n\delta^2$, where δ is the overlap between the particle and wall. The stability of the integration method was tested by using the same series of time steps as in the previous example.

The norms of the difference between total energy and initial energy for different time steps are shown in Fig. 10a. The discontinuous nature of the contact force results in a drop in accuracy for both the velocity-Verlet and second-order variational integrator, however both still out perform the first-order method. The total energy is the sum of the kinetic energy and potential energy of the Hookean contact. The total energy of the particle is plotted in Fig. 10b for $h \approx t_c/160 \approx 0.013\sqrt{m/h}$. The simulation is carried out over 250 collisions, but the graph shows the total energy for the last few collisions. The total energy of the simulation is not conserved exactly using either LAMMPS or the second-order variational integrator, but remains bounded.

3.3. Impact with a bonded pair

A simple bonded particle contact model is implemented by allowing attractive forces between particles. This is implemented by creating a 'bond' between particles if in the initial configuration they are close together ($|\delta_{ij}| < d/100$). Whenever a bond exists between particles, the potential $V_{ij} = k_n[\delta_{ij}]^2/2$ was used even when particles were separated.

A simulation is performed of a collision between a pair of bonded particles and a third unbonded particle. The purpose of this is to test the simplified bonded particle model and test the integrator with contact models that have different time scales. Different time scales can be introduced by choosing different spring stiffness constants for regular Hookean interactions (k) and bonded contacts (k_B).

The initial setup is similar to the two particle impact simulation, except that one of the particles is replaced by a bonded pair, see Fig. 11. The bonded particles are given the same initial velocity.

The bond between the two particles on the left prevents them from separating after the impact, Fig. 11a shows the particles and their trajectories after the collision. The magnitudes of two inter-particle forces are shown in Fig. 11b. The collision between particles 1 and 2 produces a peak at the impact. After the collision, the bond produces an oscillation in the force between particles 1 and 3. The maximum integration time step size is determined by the smallest time scale ($\min\{\sqrt{2k/m}, \sqrt{2k_B/m}\}$).

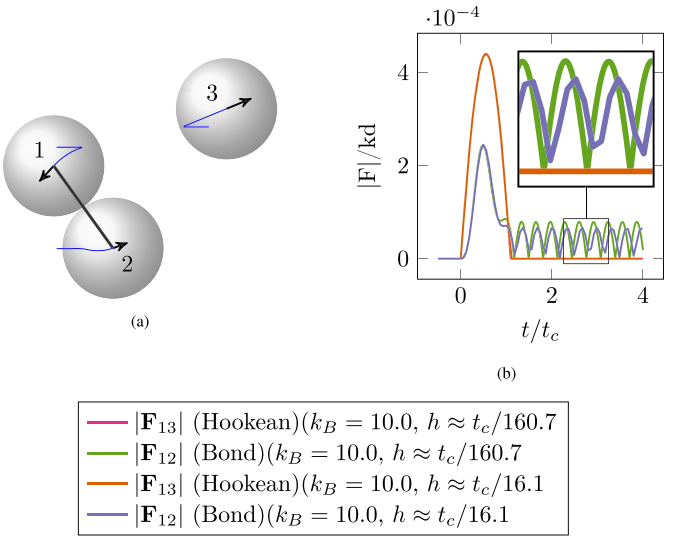

Fig. 11. Impact with a bonded pair: the configuration of particles (a) before and (b) after the collision. The trajectories of the particles are denoted by blue lines. The inter-particle forces are compared in (c), particles 1 and 2 experience a force due to the bond between them and a Hookean contact force is present momentarily between 1 and 3.

3.4. Filling a box

To investigate a less academic test case, the variational integration scheme is employed to simulate an ensemble of particles. A LAMMPS simulation was run to create an initial condition consisting of $N_p = 218$ particles in a $L \times L \times 20L$ (with $L = 6d$) box. A gravitational force was applied in the $[0, 0, -1]$ direction A snapshot of the simulation captured before all the particles had settled in the bottom of the box was used as the starting configuration of further tests. The simulation was continued in LAMMPS and the variational integrator until all the particles settled at the bottom of the box.

When making comparisons between simulations with ensembles of particles, the sensitivity of these systems to initial conditions and small numerical errors must be kept in mind. Instead of focusing on individual particle positions and velocities, macroscopic quantities are compared. Here, the average kinetic energy per particle and velocity fluctuation (which is related to the granular temperature) of the ensemble are shown as the simulation progress. These quantities are calculated as

$$\bar{K} = \frac{1}{2N_p} \sum_{i=1}^{N_P} \left\{ m \left[[v_x^i]^2 + [v_y^i]^2 + [v_z^i]^2 \right] + I \left[\omega_x^2 + \omega_y^2 + \omega_z^2 \right] \right\}, \tag{35}$$

$$\delta v = \frac{1}{3N_P} \sum_{i=1}^{N_P} \left[[\bar{v}_x - v_x^i]^2 + [\bar{v}_y - v_y^i]^2 + [\bar{v}_z - v_z^i]^2 \right], \tag{36}$$

where bars denote average velocity components: $\bar{v}_x = \sum_i^{N_P} v_x^i / N_P$.

The results are presented in Fig. 12 as a function of the simulation time. A particle system such as this is known to be sensitive to initial conditions and numerical errors, so particle trajectories diverge after a few collisions even for the same integration method with different time steps. However, the physically meaningful values such as the coarse-grained statistical quantities presented show excellent agreement with LAMMPS.

4. Conclusion

A variational integrator for DEM has been described and implemented for the Hookean contact model. Our implicit scheme has been compared against the velocity-Verlet method implemented in LAMMPS. Excellent accuracy has been observed when integrating over a single collision, and at the macro scale (particles setting in box), in addition to good long-term stability (particle bouncing between walls). A simplified bonded particle model has been implemented, thereby demonstrating the method's versatility and the ability to include other contact models. The stability of the integrator for different time steps has been compared to the velocity-Verlet method. Variational integrators have been largely overlooked for use in the Discrete Element Method, but may offer advantages over the velocity-Verlet method. In granular systems it is desirable to choose a maximal integration time step. The scaling analysis shows that variational integrators provide better stability and energy conservation, when compared to explicit methods, for granular systems with bonded particle models or in regimes characterised by long duration contacts.

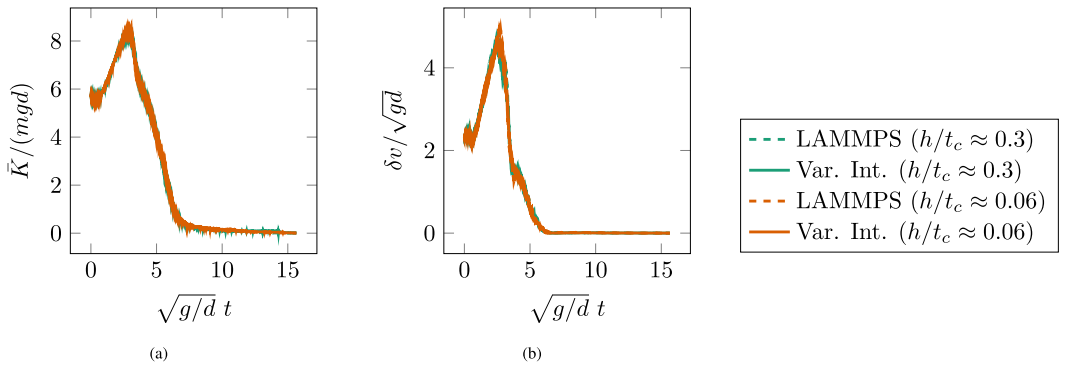

Fig. 12. Macroscopic quantities (a) kinetic energy and (b) kinetic stress of $N_p = 218$ particles settling in a box under gravity.

Using an implicit numerical method, there is additional computational expense when compared to explicit methods. However, as a variational integrator our approach is attractive since it is a discrete realisation of the Lagrange-d'Alembert principle, an extension of Hamilton's principle to non-conservative systems, that computes the trajectories of particles by finding the stationary point of the action. Therefore, it represents a dynamical extension of the atomistic simulations based on the quasi-static energy minimisation principle that inspired the Quasicontinuum (QC) method. Thus, in a fully realised granular QC method, as motivated in Fig. 1, the computational cost of using an implicit integration scheme will be offset by the reduced degrees of freedom of the simulation. Indeed, in our future work will focus on developing a suitable granular QC method, including appropriate summation rules.

CRediT authorship contribution statement

David N. De Klerk: Investigation, Software, Validation, Writing – original draft. **Thomas Shire:** Investigation, Visualization, Writing – review & editing. **Zhiwei Gao:** Investigation, Writing – review & editing. **Andrew T. McBride:** Investigation, Writing – review & editing. **Christopher J. Pearce:** Funding acquisition. **Paul Steinmann:** Conceptualization, Funding acquisition, Investigation, Writing – review & editing.

Declaration of competing interest

The authors declare that they have no known competing financial interests or personal relationships that could have appeared to influence the work reported in this paper.

Acknowledgements

This work was supported by the UK Engineering and Physical Sciences Research Council grant EP/R008531/1 for the Glasgow Computational Engineering Centre.

Appendix A. Supplementary material

Supplementary material related to this article can be found online at https://doi.org/10.1016/j.jcp.2022.111253.

References

[1] P.A. Cundall, O.D.L. Strack, A discrete numerical model for granular assemblies, Geotechnique 29 (1979) 47–65.
[2] M. Babic, Average balance equations for granular materials, Int. J. Eng. Sci. 35 (1997) 523–548.
[3] C. Miehe, J. Dettmar, A framework for micro-macro transitions in periodic particle aggregates of granular materials, Comput. Methods Appl. Mech. Eng. 193 (2004) 225–256.
[4] H.M. Jaeger, S.R. Nagel, R.P. Behringer, Granular solids, liquids, and gases, Rev. Mod. Phys. 68 (1996) 1259–1273.
[5] GDR MiDi, On dense granular flows, Eur. Phys. J. E, Soft Matter 14 (2004) 341–365.
[6] F. Da Cruz, S. Emam, M. Prochnow, J.-N. Roux, F. Chevoir, Rheophysics of dense granular materials: discrete simulation of plane shear flows, Phys. Rev. E 72 (2005) 021309.
[7] P. Jop, Y. Forterre, O. Pouliquen, A constitutive law for dense granular flows, Nature 441 (2006) 727–730.
[8] P. Jop, Rheological properties of dense granular flows, C. R. Phys. 16 (2015) 62–72.
[9] K. Kamrin, Non-locality in granular flow: phenomenology and modeling approaches, Front. Phys. 7 (2019) 116.
[10] Z. Gao, J. Zhao, Strain localization and fabric evolution in sand, Int. J. Solids Struct. 50 (2013) 3634–3648.
[11] E.B. Tadmor, M. Ortiz, R. Phillips, Quasicontinuum analysis of defects in solids, Philos. Mag. A 73 (1996) 1529–1563.
[12] J. Knap, M. Ortiz, An analysis of the quasicontinuum method, J. Mech. Phys. Solids 49 (2001) 1899–1923.
[13] R.E. Miller, E.B. Tadmor, The Quasicontinuum Method: overview, applications and current directions, J. Comput.-Aided Mater. Des. 9 (2002) 203–239.

[14] E.B. Tadmor, R.E. Miller, The theory and implementation of the Quasicontinuum Method, in: S. Yip (Ed.), Handb. Mater. Model., Springer Netherlands, Dordrecht, 2005, pp. 663–682.
[15] D.M. Kochmann, G.N. Venturini, A meshless quasicontinuum method based on local maximum-entropy interpolation, Model. Simul. Mater. Sci. Eng. 22 (2014) 034007.
[16] J.S. Amelang, G.N. Venturini, D.M. Kochmann, Summation rules for a fully nonlocal energy-based quasicontinuum method, J. Mech. Phys. Solids 82 (2015) 378–413.
[17] J.E. Marsden, S. Pekarsky, S. Shkoller, Discrete Euler-Poincaré and Lie-Poisson equations, Nonlinearity 12 (1999) 1647–1662.
[18] C. Kane, J.E. Marsden, M. Ortiz, M. West, Variational integrators and the Newmark algorithm for conservative and dissipative mechanical systems, Int. J. Numer. Methods Eng. 49 (2000) 1295–1325.
[19] J.E. Marsden, M. West, Discrete mechanics and variational integrators, Acta Numer. 10 (2001) 357–514.
[20] A. Lew, J.E. Marsden, M. Ortiz, M. West, An overview of variational integrators, in: A.M.L.P. Franca, T.E. Tezduyar (Eds.), Finite Elem. Methods 1970's Beyond, International Center for Numerical Methods in Engineering (CIMNE), Barcelona, 2004, https://resolver.caltech.edu/CaltechAUTHORS:20101005-091206576.
[21] A. Lew, J.E. Marsden, M. Ortiz, M. West, Variational time integrators, Int. J. Numer. Methods Eng. 60 (2004) 153–212.
[22] M. Vermeeren, A. Bravetti, M. Seri, Contact variational integrators, J. Phys. A, Math. Theor. 52 (2019) 1–29.
[23] L. Verlet, Computer "experiments" on classical fluids. I. Thermodynamical properties of Lennard-Jones molecules, Phys. Rev. 159 (1967) 98–103.
[24] E. Hairer, C. Lubich, G. Wanner, Geometric numerical integration illustrated by the Störmer–Verlet method, Acta Numer. 12 (2003) 399–450.
[25] R. Ruth, A canonical integration technique, IEEE Trans. Nucl. Sci. 30 (1983) 2669–2671.
[26] B.J. Leimkuhler, R.D. Skeel, Symplectic numerical integrators in constrained Hamiltonian systems, J. Comput. Phys. 112 (1994) 117–125.
[27] C. O'Sullivan, J.D. Bray, Selecting a suitable time step for discrete element simulations that use the central difference time integration scheme, Eng. Comput. 21 (2004) 278–303.
[28] K. Washino, E.L. Chan, K. Miyazaki, T. Tsuji, T. Tanaka, Time step criteria in DEM simulation of wet particles in viscosity dominant systems, Powder Technol. 302 (2016) 100–107.
[29] M. Otsubo, C. O'Sullivan, T. Shire, Empirical assessment of the critical time increment in explicit particulate discrete element method simulations, Comput. Geotech. 86 (2017) 67–79.
[30] T.C. Ke, J. Bray, Modeling of particulate media using discontinuous deformation analysis, J. Eng. Mech. 121 (1995) 1234–1243.
[31] K. Samiei, B. Peters, M. Bolten, A. Frommer, Assessment of the potentials of implicit integration method in discrete element modelling of granular matter, Comput. Chem. Eng. 49 (2013) 183–193.
[32] D. Krijgsman, S. Luding, Simulating granular materials by energy minimization, Comput. Part. Mech. 3 (2016) 463–475.
[33] J. Rojek, Contact modeling in the Discrete Element Method, in: A. Popp, P. Wriggers (Eds.), Contact Model. Solids Part., vol. 585, Springer International Publishing, 2018, pp. 177–228.
[34] L.E. Silbert, D. Ertaş, G.S. Grest, T.C. Halsey, D. Levine, S.J. Plimpton, Granular flow down an inclined plane: Bagnold scaling and rheology, Phys. Rev. E 64 (2001) 051302.
[35] Python Software Foundation, Python Language Reference version 3.8.5, www.python.org, 2020.
[36] G. Van Rossum, Python Tutorial, Technical Report, Centrum voor Wiskunde en Informatica (CWI), Amsterdam, 1994.
[37] D. De Klerk, T. Shire, Z. Gao, A. McBride, C. Pearce, P. Steinmann, A variational integrator for the Discrete Element Method: companion code, https://doi.org/10.5281/zenodo.5752185, 2021.
[38] S. Plimpton, Fast parallel algorithms for short-range molecular dynamics, J. Comput. Phys. 117 (1995) 1–19.
[39] N.V. Brilliantov, F. Spahn, J.-M. Hertzsch, T. Pöschel, Model for collisions in granular gases, Phys. Rev. E 53 (1996) 5382–5392.
[40] H.P. Zhang, H.A. Makse, Jamming transition in emulsions and granular materials, Phys. Rev. E 72 (2005) 011301.
[41] K.J. Hanley, C. O'Sullivan, Analytical study of the accuracy of discrete element simulations, Int. J. Numer. Methods Eng. 109 (2017) 29–51.
[42] M. Tuckerman, B.J. Berne, G.J. Martyna, Reversible multiple time scale molecular dynamics, J. Chem. Phys. 97 (1992) 1990–2001.
[43] R.D. Skeel, G. Zhang, T. Schlick, A family of symplectic integrators: stability, accuracy, and molecular dynamics applications, SIAM J. Sci. Comput. 18 (1997) 203–222.